2,6-bis(5-(*tert*-butyl)-1*H*-pyrazol-3-yl)pyridine. Effects of the Peripheral Aliphatic Side Chain on the Coordination of Actinides(III) and Lanthanides(III).

Jonas Stracke,[a,b] Patrik Weßling,[b] Thomas Sittel,[a] Christian Adam,[a] Frank Rominger,[c] Andreas Geist,[a] and Petra J. Panak.[a,b]

[a]Karlsruhe Institute of Technology (KIT), Institute for Nuclear Waste Disposal (INE), P.O. Box 3640, 76021 Karlsruhe, Germany

[b]Heidelberg University, Institut für Physikalische Chemie, Im Neuenheimer Feld 253, 69120 Heidelberg, Germany

[c]Heidelberg University, Institut für Organische Chemie, Im Neuenheimer Feld 270, 69120 Heidelberg, Germany

KEYWORDS: Actinides, Lanthanides, Lipophilic ligands, Complexation, Selectivity.

ABSTRACT

To improve the understanding of the interaction mechanism in trivalent lanthanide and actinide complexes, studies with structurally different hard and soft donor ligands are of great interest. For that reason, the coordination chemistry of An(III) and Ln(III) with 2,6-bis(5-(*tert*-butyl)-1*H*-pyrazol-3-yl)pyridine (C4-BPP) has been explored. Time-resolved laser fluorescence spectroscopy (TRLFS) studies have revealed the formation of $[Cm(C4\text{-}BPP)_n]^{3+}$ (n = 1-3) ($\log \beta'_1 = 7.2 \pm 0.4$, $\log \beta'_2 = 10.1 \pm 0.5$ and $\log \beta'_3 = 11.8 \pm 0.6$) and $[Eu(C4\text{-}BPP)_m]^{3+}$ (m = 1-2) ($\log \beta'_1 = 4.9 \pm 0.2$ and $\log \beta'_2 = 8.0 \pm 0.4$). The absence of the $[Eu(C4\text{-}BPP)_3]^{3+}$ complex shows a more favorable complexation of Cm(III) over Eu(III). Additionally, complementary NMR measurements have been conducted to examine the M(III)-N bond in Ln(III) and Am(III) C4-BPP complexes. ^{15}N-NMR data have revealed notable differences in the chemical shifts of the coordinating nitrogen atoms between the Am(III) and Ln(III) complexes. In the Am(III) complex, the coordinating nitrogen atoms have shown a shift by 260 ppm, indicating a higher fraction of covalent bonding in the Am(III)-N bond compared to the Ln(III)-N bond. This observation aligns excellently with the differences in stability constants obtained from TRLFS studies.

INTRODUCTION

Liquid-liquid extraction represents a widely used and successfully applied method to separate dissolved ionic species from each other.[1-4] However, the separation of trivalent actinides (An) and lanthanides (Ln) using liquid-liquid extraction is challenging due to their characteristic chemical similarity.[5] However, the required selectivity can be achieved with ligands containing soft donor atoms such as sulfur[6, 7] or nitrogen[8, 9]. While sulfur containing ligands are only of marginal importance due to problems with disposal, mainly heterocyclic ligands with nitrogen donor atoms such as bis(triazinyl)pyridines (BTPs) or bis(triazinyl)bipyridines (BTBPs) have proven to be highly efficient extractants for the selective complexation and extraction of An(III) over Ln(III) (Figure 1).[4, 10-12] For example ^{n}Pr-BTP shows an $SF_{Am/Eu} \approx 100$.[8] Additionally, the stability constant of $[Cm(^{n}Pr\text{-}BTP)_3]^{3+}$ ($\log \beta'_3 = 17.4 \pm 0.4$) is nearly three orders of magnitude larger than of $[Eu(^{n}Pr\text{-}BTP)_3]^{3+}$ ($\log \beta'_3 = 14.7 \pm 0.4$).[13] The chemical background for the observed selectivity of these ligands is not yet well understood.[14, 15] However, it is suggested that the selectivity is due to differences in the bonding mode, namely a higher covalent bond fraction, between An(III) and ligand compared to Ln(III) and ligand.[14-18]

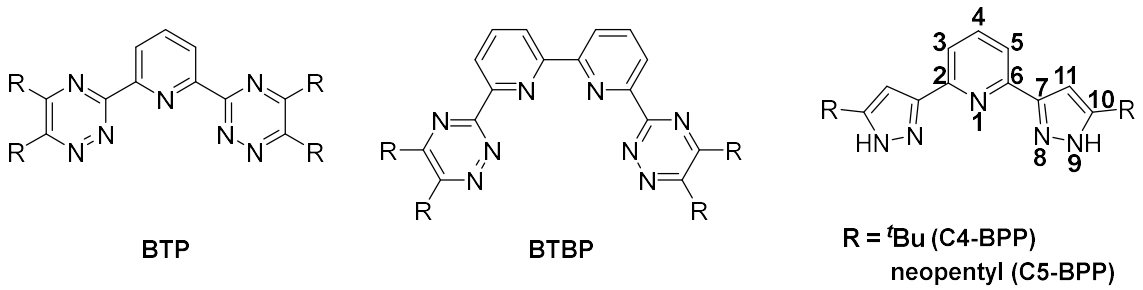

Figure 1: General structural motifs of BTP (left), BTBP (center) and BPP (right).

This difference in the bonding mode is proven by an ^{15}NMR shift up to 360 ppm in the Am(III) complex of the coordinating nitrogen atoms in respect to the non-coordinating ones and the corresponding Ln(III) complexes. [19] Supplementary to elaborate studies on BTPs and BTBPs, various ligands have been investigated to clarify their selectivity by variation of their aromatic backbones systematically.[20-22] For instance, replacing the triazinyl groups of the BTP with pyrazolyl rings results in the ligand 2,6-bis(5-(2,2-dimethylpropyl)-1*H*-pyrazol-3-yl)pyridine (C5-BPP) (Figure 1).[11] Furthermore the variation of the sidechain also results in large deviations of the properties of these ligands. For example the difference between the stability constants of $[Cm(^{i}Pr\text{-}BTP)_3]^{3+}$ ($\log \beta_3' = 16.3 \pm 0.3$) and $[Cm(^{n}Pr\text{-}BTP)_3]^{3+}$ ($\log \beta_3' = 14.4 \pm 0.3$) is two orders of magnitude.[23] According to this result, the neopentyl group of C5-BPP was exchanged by a ^{t}butyl group (C4-BPP). Then, Ln(III) and An(III) complexes were prepared and characterized by various analytical methods to determine the complexation properties of this new ligand in comparison to C5-BPP.

EXPERIMENTAL SECTION

NMR Sample Preparation. C4-BPP (3.00-6.00 eq), dissolved in 600 µL of deuterated methanol, was added to 1.00 eq of the metal triflate (Y, La, Sm, Lu). The obtained solution was transferred into an NMR tube. Chemical shifts are given in ppm and coupling constants in Hz. ^{1}H- and ^{13}C-specta were calibrated in relation to deuterated solvents. Am sample: 4.7 mg of C4-BPP (14.4 mmol) was dissolved in 600 µL of deuterated methanol. This was added to the evaporation residue of the $^{243}Am(OTf)_3$ solution containing 1 mg of ^{243}Am(III). The solution was then transferred into a J. Young-type NMR tube.[24-26]

NMR Titration. For the NMR titration experiments the ligand solution was prepared by dissolving C4-BPP (6.00 eq, 19.4 mg, 60 µmol) in 360 µL of deuterated methanol thus obtaining a 0.167 M C4-BPP solution. 1.00 eq of the metal ion (Y, La, Sm, Lu), as triflate salt, was dissolved in 450 µL of deuterated methanol in a separate vial. The metal salt solution was then transferred into an NMR tube. The ligand solution was added subsequently in 0.25 eq steps to monitor the progress of the complexation.[24-26]

NMR Measurements. NMR spectra were recorded at T = 300 K on a Bruker Avance III 400 spectrometer operating at a resonance frequency of 400.18 MHz for ^{1}H, 100.6 MHz for ^{13}C, 376.5 MHz for ^{19}F and 40.6 MHz for ^{15}N. The spectrometer was equipped with a z-gradient observe room temperature probe. Chemical shifts were referenced internally to tetramethylsilane (TMS) (δ(TMS) = 0 ppm) by the deuterium lock signal of methanol-*d*$_4$ or $CDCl_3$. ^{15}N shifts are referenced to $^{15}NH_4Cl$ with $\delta(NH_4CL)$ = 0 ppm. All 1D spectra were recorded with 32k data points and were zero filled to 64k points. ^{15}N data were obtained from ^{1}H, ^{15}N-HMBC spectra. Deuterated solvents were purchased from Euriso-Top GmbH.[2, 11, 24, 26]

TRLFS Sample Preparation. Stock solutions of C4-BPP were prepared by dissolving 85 mg in 1200 µL of methanol containing 1.5 vol.% water ($2.2 \cdot 10^{-1}$ mol/L). Solutions with lower C4-BPP concentrations were obtained through diluting with methanol containing 1.5 vol.% water. TRLFS samples were prepared by adding 4.7 µL of a Cm(III) stock solution ($2.12 \cdot 10^{-5}$ mol/L $Cm(ClO_4)_3$ in 0.1 mol/L $HClO_4$; ^{248}Cm: 89.7 %, ^{246}Cm: 9.4 %, ^{243}Cm: 0.4 %, ^{244}Cm: 0.3 %, ^{245}Cm: 0.1 %, ^{247}Cm: 0.1 %) to 985 µL of methanol and 10.3 µL water, resulting in an initial Cm(III) concentration of $1 \cdot 10^{-7}$ mol/L. Eu(III)-TRLFS samples were prepared by adding 9.4 µL of a Eu(III) stock solution ($1.07 \cdot 10^{-3}$ mol/L $Eu(ClO_4)_3$ in $1.0 \cdot 10^{-2}$ mol/L $HClO_4$ to 985 µL of methanol and 5.6 µL of water, resulting in an initial Eu(III) concentration of $1.0 \cdot 10^{-5}$ mol/L. By adding appropriate volumes of the various ligand solutions the ligand concentration was adjusted. The resulting solutions were allowed to equilibrate for 10 min before measurement. Previous kinetic studies were performed to confirm, that this time was sufficient to reach equilibrium.[2, 11, 24]

TRLS Measurements. TRLFS measurements were performed at 293 K using a Nd:YAG (Surelite II laser, Continuum) pumped dye laser system (NarrowScan D-R; Radiant Dyes Laser Accessories GmbH). Cm(III) was exited at a wavelength of 396.6 nm. Eu(III) was exited at a wavelength of 394.0 nm. A spectrograph (Shamrock 303i, ANDOR) with 300, 1199 and 2400 lines per millimeter gratings was used for spectral decomposition. The detection of the fluorescence emission was performed using an ICCD camera (iStar Gen III; ANDOR). To discriminate short-lived organic fluorescence and light scattering a delaytime of 1 µs was set.[2, 11]

X-ray Crystallographic Studies. Crystals of $[Eu(C4\text{-}BPP)(H_2O)_4(DMF)_2]Cl_3$ were obtained from DMF/diethyl ether recrystallization. The crystal was measured on a Bruker APEX-II Quazar area detector diffractometer. The structure was resolved by direct or dual space methods (SHELXT-2018/2), and refined against F^2 with a full-matrix least-squares algorithm using SHELXT-2018/3. The hydrogen atom contributions were calculated but not refined. The residual electron densities was of no chemical significance.

Crystal Data: $C_{25}H_{39}Cl_3EuN_7O_6$, M_r = 791.94, orthorhombic, a = 21.488(3) Å, b = 8.1677(9) Å, c = 10.0164(11) Å, α = 90 °, β = 90 °, γ = 90 °, V = 1758.0(3) Å^3, T = 200(2) K, space group Imm2, Z = 2, μ(Mo Kα) = 2.057 mm-1, 12067 reflections measured, 2065 independent reflections (R_{int} = 0.0576). The final R1 value was 0.035 (I > 2σ(I)). The final $R_w(F^2)$ value was 0.067 (all data). The quality of fit on F2 was 1.09.

DFT Calculations: DFT calculations were performed with the BP86[27, 28] functional and def2-TZVP[29] basis set for the $[Cm(C4\text{-}BPP)_3]^{3+}$ complex using TURBOMOLE.[30] Cm(III) was modulated with a ECP60MWB[31] pseudo core potential. Vibration modes were calculated to confirm a true minimum of the optimized structure.[3]

VSBS: Vibronic side band detection was performed in a wavelength range of 620 nm to 800 nm with a 1199 lines per mm grating. The mentioned wavelength range was measured by gradually shifting the central wavelength in 10 nm steps, since the maximum detection width of the grating (40 nm) was exceeded.[3]

1,1'-(pyridine-2,6-diyl)bis(4,4-dimethylpentane-1,3-dione). Dimethyl 2,6-pyridinedicarboxylate (2.50 g, 12.8 mmol) and Sodium tert-butoxide (2.71 g, 28.2 mmol) was dissolved in 40 mL of dry THF. 3,3-Dimethylbutane-2-one (2.82 g, 28.2 mmol) was added dropwise and the reaction mixture was heated at 60 °C for 48 h. Subsequently, it was cooled to room temperature, the solvent was removed and water was added. The mixture was then acidified with diluted HCl until full precipitation. After filtration and washing with water the crude product was purified by flash column chromatography with PE:EA (20:1). A white solid was obtained. Yield: 1.68 g (5.1 mmol, 40 %). ^{1}H NMR (400.2 MHz, $CDCl_3$, 300 K): δ 1.30 (s, 18H, CH_3), 7.12 (s, 2H, CH), 7.99 (dd, 1H, ^{3}J = 8.0 Hz, ^{3}J = 7.7 Hz, Py H), 8.19 (d, 2H, ^{3}J = 7.8 Hz, Py H), 15.88 (s, 2H, OH) ppm.

2,6-bis(5-(tert-butyl)-1H-pyrazol-3-yl)pyridine (C4-BPP). 1.68 g of 1,1'-(pyridine-2,6-diyl)bis(4,4-dimethylpentane-1,3-dione) (5.07 mmol) was suspended in 40 ml of ethanol and 1.6 mL of hydrazine hydrate (60 % in H_2O, 30 mmol) was added. The reaction mixture was refluxed for 4 h. The solvent was removed and the residue washed with pentane. The product was obtained as a white solid. Yield: 1.68 g, 5.00 mmol, quantitative. ^{1}H NMR (400.2 MHz, $CDCl_3$, 300 K): δ 1.38 (s, 18H, H-13), 6.67 (s, 2H, H-11), 7.62-7.70 (m, 3H, H-3/5 and H-4), 9.27 (s, 2H, NH) ppm. ^{1}H NMR (400.2 MHz, methanol-*d*$_4$, 300 K): δ 1.40 (s, 18H, H-13), 6.79 (s, 2H, H-11), 7.60-7.86 (m, 3H, H-3/5 and H-4) ppm. ^{1}H NMR (400.2 MHz, methanol-*d*$_4$ + HOTf, 300 K): δ 1.46 (s, 18H, H-13), 7.11 (s, 2H, H-11), 8.14 (d, 2H, ^{3}J = 8.0 Hz, H-3/5), 8.34 (dd, 1H, ^{3}J = 8.0 Hz, H-4) ppm. ^{19}F[[^{1}H]] NMR (376.5 MHz, methanol-*d*$_4$ + HOTf, 300 K): δ -80.1 ppm. ^{13}C[[^{1}H]] NMR (100.6 MHz, methanol-*d*$_4$ + HOTf, 300 K): δ 28.82 (C13), 31.13 (C12), 101.7 (C11), 121.6 (C5), 143.3 (C4), 144.5 (C6), 146.4 (C7), 157.8 (C10) ppm. ^{15}N NMR (40.6 MHz, methanol-*d*$_4$ + HOTf, 300 K): δ 202 (N9), 230 (N1), 254 (N8) ppm.

[Y(C4-BPP)$_3$][OTf]$_3$. ^{1}H NMR (400.2 MHz, methanol-*d*$_4$, 300 K): δ 1.12 (s, 54H, H-13), 6.71 (s, 6H, H-11), 7.94 (d, 6H, ^{3}J = 7.9 Hz, H-3/5), 8.19 (t, 3H, ^{3}J = 7.9 Hz, H-4) ppm. ^{19}F[[^{1}H]] NMR (376.5 MHz, methanol-*d*$_4$, 300 K): δ -79.9 ppm. ^{13}C[[^{1}H]] NMR (100.6 MHz, methanol-*d*$_4$, 300 K): δ 28.61 (C13), 30.81 (C12), 100.8 (C11), 121.6 (C5), 141.6 (C4), 149.0 (C6), 152.2 (C7), 159.1 (C10) ppm. ^{15}N NMR (40.6 MHz, methanol-*d*$_4$, 300 K): δ 200 (N9), 263 (N1), 265 (N8) ppm.

[La(C4-BPP)$_3$][OTf]$_3$. ^{1}H NMR (400.2 MHz, methanol-*d*$_4$, 300 K): δ 1.14 (s, 54H, H-13), 6.69 (s, 6H, H-11), 7.95 (d, 6H, ^{3}J = 7.7 Hz, H-3/5), 8.18 (t, 3H, ^{3}J = 7.7 Hz, H-4) ppm. ^{19}F[[^{1}H]] NMR (376.5 MHz, methanol-*d*$_4$, 300 K): δ -79.9 ppm. ^{13}C[[^{1}H]] NMR (100.6 MHz, methanol-*d*$_4$, 300 K): δ 28.65 (C13), 30.74 (C12), 101.1 (C11), 121.9 (C5), 141.6 (C4), 150.5 (C6), 152.4 (C7), 158.2 (C10) ppm.

[Sm(C4-BPP)$_3$][OTf]$_3$. ^{1}H NMR (400.2 MHz, methanol-d_4, 300 K): δ 1.19 (s, 54H, H-13), 7.12 (s, 6H, H-11), 8.44 (d, 6H, ^{3}J = 7.8 Hz, H-3/5), 8.58 (t, 3H, ^{3}J = 7.8 Hz, H-4) ppm. ^{19}F[[^{1}H]] NMR (376.5 MHz, methanol-d_4, 300 K): δ -79.9 ppm. ^{13}C[[^{1}H]] NMR (100.6 MHz, methanol-d_4, 300 K): δ 28.66 (C13), 30.82 (C12), 101.3 (C11), 121.6 (C5), 142.4 (C4), 153.7 (C6), 155.1 (C7), 158.4 (C10) ppm. ^{15}N NMR (40.6 MHz, methanol-d_4, 300 K): δ 200 (N9), 218 (N1), 224 (N8) ppm.

[Lu(C4-BPP)$_3$][OTf]$_3$. ^{1}H NMR (400.2 MHz, methanol-d_4, 300 K): δ 1.11 (s, 54H, H-13), 6.73 (s, 6H, H-11), 7.95 (d, 6H, ^{3}J = 7.9 Hz, H-3/5), 8.20 (t, 3H, ^{3}J = 7.9 Hz, H-4) ppm. ^{19}F[[^{1}H]] NMR (376.5 MHz, methanol-d_4, 300 K): δ -79.9 ppm.^{13}C[[^{1}H]] NMR (100.6 MHz, methanol-d_4, 300 K): δ 28.59 (C13), 30.82 (C12), 100.9 (C11), 121.6 (C5), 141.6 (C4), 148.7 (C6), 152.4 (C7), 159.4 (C10) ppm. ^{15}N NMR (40.6 MHz, methanol-d_4, 300 K): δ 200 (N9), 265 (N1), 267 (N8) ppm.

[Am(C4-BPP)$_3$][OTf]$_3$. ^{1}H NMR (400.2 MHz, methanol-d_4, 300 K): δ 1.10 (s, 54H, H-13), 6.09 (s, 6H, H-11), 7.39 (dd, 3H, ^{3}J = 7.6 Hz, ^{3}J = 7.5 Hz, H-4), 7.95 (d, 6H, ^{3}J = 7.9 Hz, H-3/5) ppm. ^{19}F[[^{1}H]] NMR (376.5 MHz, methanol-d_4, 300 K): δ -79.9 ppm. ^{15}N NMR (40.6 MHz, methanol-d_4, 300 K): δ 210 (N9), -3 (N1), -6 (N8), 13 (N8 of *[Am(C4-BPP)][OTf]$_3$*) ppm.

RESULTS AND DISCUSSION

Ligand Synthesis. C4-BPP is synthesized in two steps (Figure 2) starting with dimethyl 2,6-pyridinedicarboxylate (1). In a Claisen condensation the dimethyl ester is treated with 3,3-dimethylbutane-2-one in the presence of sodium tert-butoxide. This lead to the corresponding β-diketone (2). Addition of hydrazine-hydrate solution in ethanol results in the desired product C4-BPP with a total yield of 40 %. The purity of C4-BPP is confirmed by ^{1}H and $^{13}C[[^{1}H]]$ NMR spectroscopy.

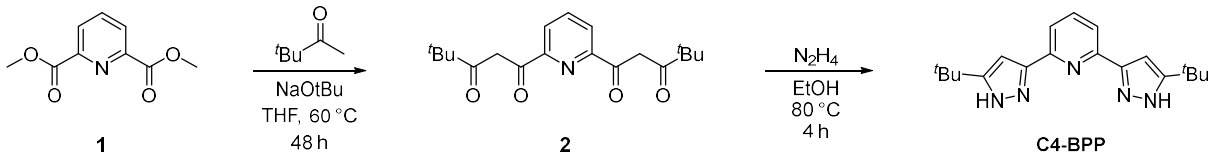

Figure 2: Synthesis of C4-BPP.

Eu(III) Complex Structure. The resemblance between C4-BPP and C5-BPP raises the question if their bonding properties towards An(III) and Ln(III) are the same in comparable complexes. For this reason, $[Eu(C4\text{-}BPP)_n]^{3+}$ is crystallized and analyzed by x-ray diffraction. The complex is obtained (according to Figure 3) as light brown crystals, which contain additionally coordinated water and DMF molecules in the first coordination sphere (Figure 4). This indicates the inability of C4-BPP to fully displace the solvent molecules under the given conditions, as already observed for C5-BPP. [11]

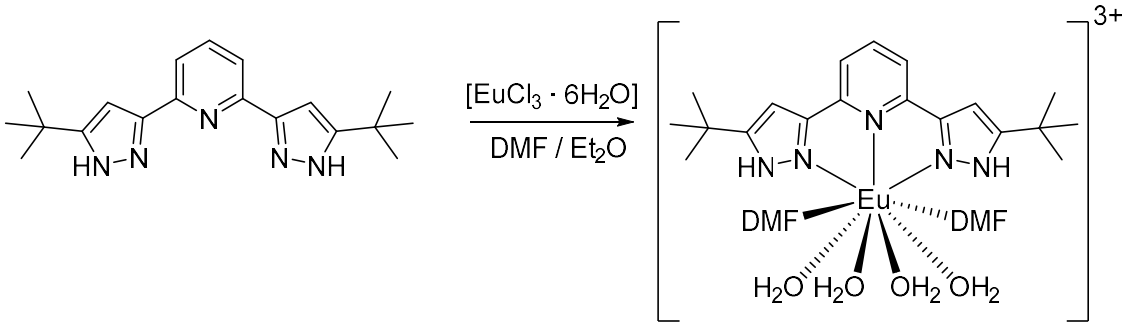

Figure 3: Synthesis of $[Eu(C4\text{-}BPP)(H_2O)_4(DMF)_2]Cl_3$.

$[Eu(C4\text{-}BPP)(H_2O)_4DMF_2]Cl_3$ crystallizes in an orthorhombic space group Imm2 and has two molecules of the complex per unit cell. Eu(III) is nine fold coordinated by four water molecules, two DMF molecules and the tridentate C4-BPP forming a square face monocapped antiprism (Supporting Information; Figure 1).

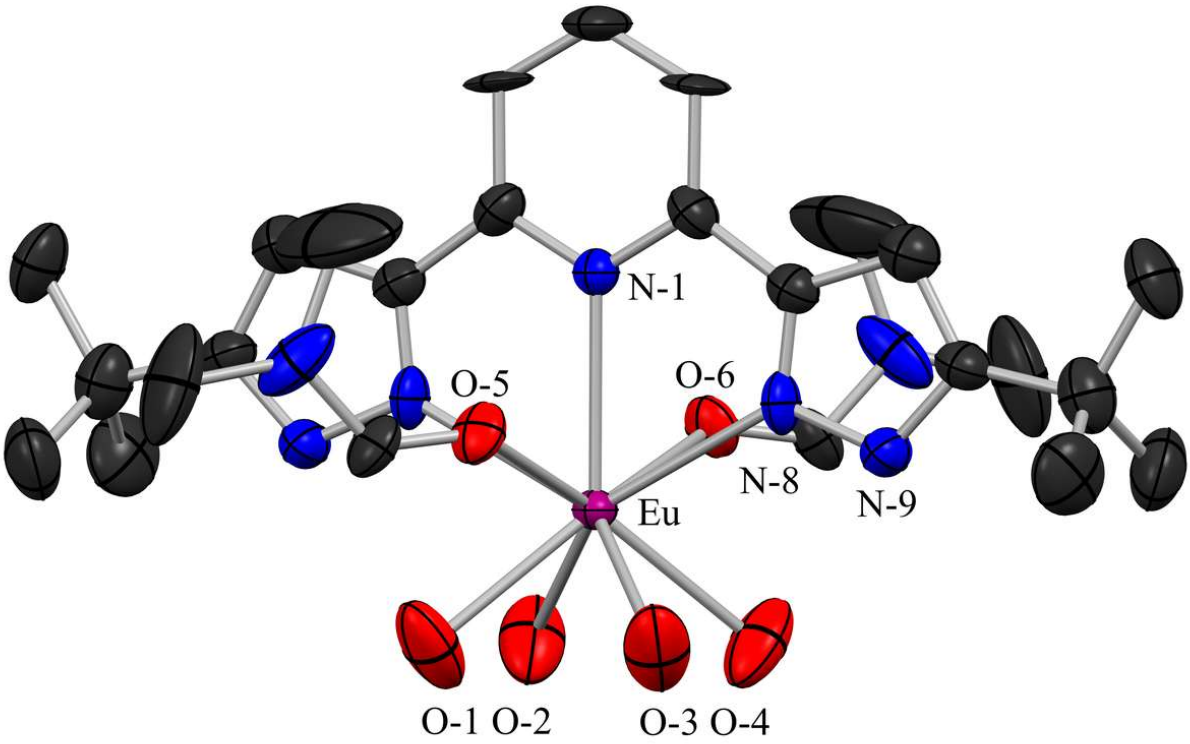

Figure 4: Solid state structure of $[Eu(C4\text{-}BPP)(H_2O)_4DMF_2]Cl_3$ showing the atom-labelling scheme, omitting hydrogen atoms. Thermal ellipsoids show a probability of 50 %. Selected bond lengths (Å) and angles (deg): Eu-O1 = 2.457(5), Eu-O2 = 2.457(5), Eu-O3 = 2.457(5), Eu-O4 = 2.457(5), Eu-O5 = 2.444(8), Eu-O6 = 2.444(8), Eu-N1 = 2.622(10), Eu-N8 = 2.537(8), Eu-N8‘ = 2.537 (8); N1-Eu-N8 = 61.61(19), N8-Eu-N8‘ = 123.2(4), N1-Eu-N8‘ = 61.61(19).

Comparing the structures of Eu-C5-BPP and Eu-C4-BPP complexes, the most significant characteristics of both complexes are represented by their bond lengths between the coordinated nitrogen atoms and the central metal ion (N1, N8 and N8';Figure 4, Table 1). Despite the slight differences regarding the two complexes' inner coordination spheres, the Eu-N bond lengths agree very well within uncertainties.

Table 1: Selected bond lengths (Å) of $[Eu(C4\text{-}BPP)(H_2O)_4DMF_2]Cl_3$ (Figure 4) and $[Eu(C5\text{-}BPP)(\eta^2\text{-}NO_3)_3DMF]$.[11]

	Eu-N1 [Å]	**Eu-N8 [Å]**	**Eu-N8‘ [Å]**
$[Eu(C4\text{-}BPP)(H_2O)_4DMF_2]Cl_3$	2.622(10)	2.537(8)	2.537 (8)
$[Eu(C5\text{-}BPP)(\eta^2\text{-}NO_3)_3DMF]$	2.622(4)	2.545(4)	2.541(5)

Speciation studies of Cm(III) with C4-BPP. TRLFS is utilized to investigate the speciation of Cm(III) and Eu(III) with C4-BPP in solution. Cm(III) is dissolved in methanol containing 1.5 vol.% water and the concentration of C4-BPP is gradually increased. The normalized emission spectra resulting from the $^6D'_{7/2} \rightarrow {}^8S'_{7/2}$ transition are shown in Figure 5.

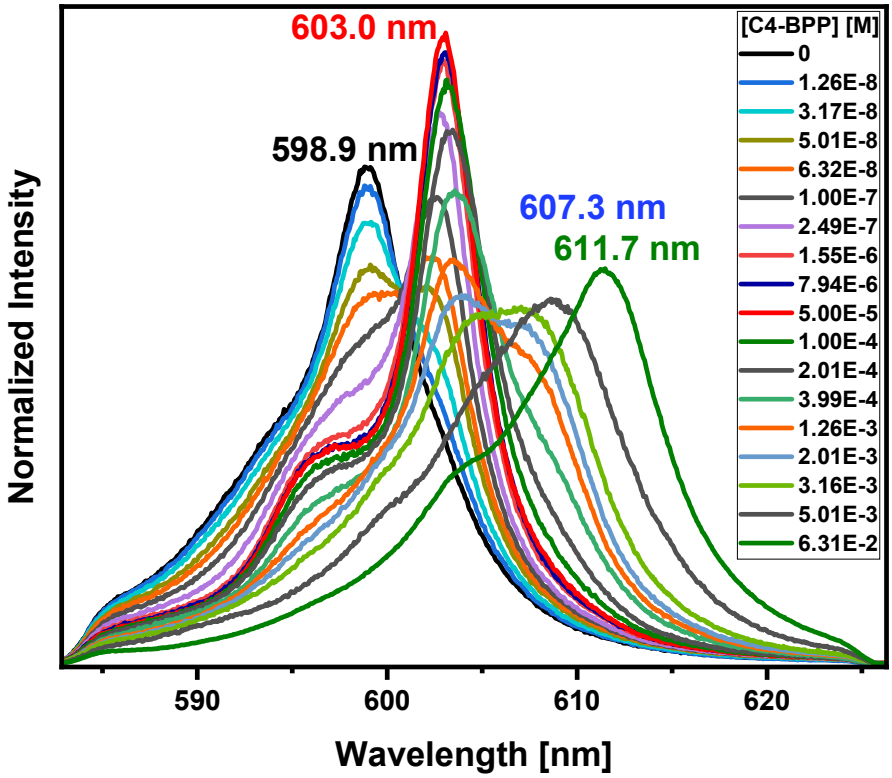

Figure 5: Normalized fluorescence spectra of Cm(III) in methanol containing 1.5 vol.% water as a function of the C4-BPP concentration. $[Cm(III)]_{ini} = 1.0 \bullet 10^{-7}$ mol/L, [C4-BPP] = (0 - 6.31) • 10^{-2} mol/L.

In absence of C4-BPP the solvent spectrum of Cm(III) in methanol containing 1.5 vol.% water shows an emission band at 598.9 nm (Figure 5). The spectrum displays a bathochromic shift compared to the Cm(III) aquo ion $[Cm(H_2O)_9]^{3+}$, located at 593.8 nm.[32, 33] This results from the partial exchange of water molecules by methanol molecules in the first coordination sphere. The lifetime of 131 ± 7 µs and the position of the emission band are in agreement with the literature (Figure S2).[11] With increasing C4-BPP concentration a bathochromic shift of the emission band is observed. This originates from the increased splitting of the $^6D'_{7/2}$ state resulting from the complexation of Cm(III) with C4-BPP.[34, 35] Three new emissions bands at 603.0, 607.3 and 611.7 nm are observed. Due to the resemblance with the emission spectra of C5-BPP, the bands are assigned to $[Cm(C4\text{-}BPP)_n]^{3+}$ (n = 1-3) respectively[11]. The fluorescence lifetime of the sample with the highest ligand concentration – 535 ± 27 µs – further confirms the formation of the $[Cm(C4\text{-}BPP)_3]^{3+}$ complex (Figure S2). The Cm(III) species distribution is derived by peak deconvolution of the fluorescence spectra (Figure 5). The single component spectra (Figure S3) are used to perform the peak deconvolution (for further details on peak deconvolution, see references).[2, 3]

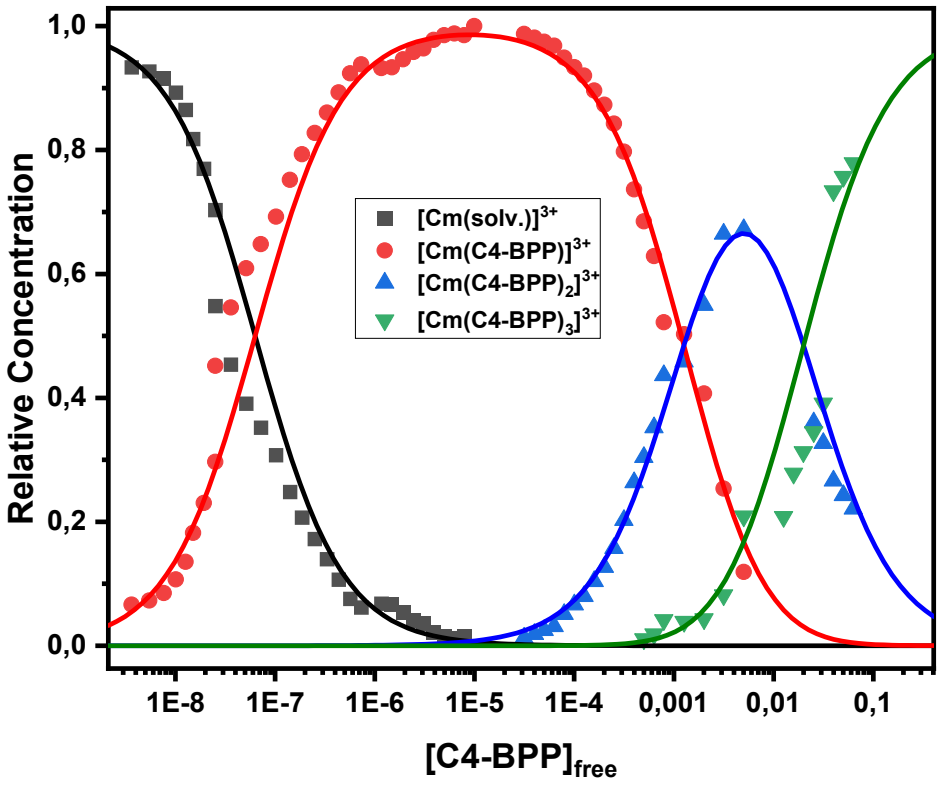

Figure 6: Relative Cm(III) species concentrations in methanol containing 1.5 vol.% water as a function of the free C4-BPP concentration. Symbols denote experimental data, while lines are calculated using log β'_1 = 7.2, log β'_2 = 10.1 and log β'_3 = 11.8. T = 293 K.

As shown in Figure 6, the formation of the 1:1 complex, $[Cm(C4\text{-}BPP)]^{3+}$, starts at a C4-BPP concentration of less than 10^{-8} mol/L and is the only species present at C4-BPP concentrations around 10^{-5} mol/L. The 1:2 complex, $[Cm(C4\text{-}BPP)_2]^{3+}$, starts forming at a C4-BPP concentration of 10^{-5} mol/L, with a maximum share of 65% at a C4-BPP concentration of 5 mmol/L. Finally, for C4-BPP concentrations of $5.0 \cdot 10^{-4}$ mol/L, the formation of the 1:3 complex, $[Cm(C4\text{-}BPP)_3]^{3+}$, is observed. Based on the evolution of the Cm(III) spectra a stepwise complexation model according to equation (1) is assumed (L = C4-BPP, M = Cm). [11]

$$[ML_{n-1}]^{3+} + L \rightleftharpoons [ML_n]^{3+} \qquad (n = 1 - 3) \tag{1}$$

The correlation between the logarithm of $[Cm(C4\text{-}BPP)_n]^{3+}/[Cm(C4\text{-}BPP)_{n-1}]^{3+}$ (n = 1-3) and the logarithm of the free C4-BPP concentration is depicted in the supporting information (Figure 4). The stepwise complexation model assumes a slope of one. According to equation (2) the linear regression yields slopes

of 1.05 ± 0.05, 0.99 ± 0.06 and 0.94 ± 0.04 for the formation of the $[Cm(C4\text{-}BPP)_n]^{3+}$ complexes (n = 1-3), respectively.

$$\log\left(\frac{[M(L)_n]^{3+}}{[M(L)_{n-1}]^{3+}}\right) = \log K'_n + n \cdot \log\left([L]_{free}\right) \quad \textbf{(2)}$$

This verifies the assumed complexation model and the correct assignment of the $[Cm(C4\text{-}BPP)_n]$ (n =1-3) complexes. The conditional stability constants are calculated with equations (3). The values are shown in Table 2.

$$\beta'_n = \frac{[M(L)_n]^{3+}}{[M]^{3+} \cdot [L]^n_{free}} \quad \textbf{(3)}$$

Table 2: Stability constants of C4-BPP and C5-BPP for Cm(III) in methanol containing 1.5 vol.% water.[11]

	log β'$_1$ (Cm(III))	**log β'$_2$ (Cm(III))**	**log β'$_3$ (Cm(III))**
C4-BPP	7.2 ± 0.4	10.1 ± 0.5	11.8 ± 0.6
C5-BPP	6.9 ± 0.2	11.2 ± 0.3	14.8 ± 0.4

Comparing the conditional stability constants of C5-BPP and C4-BPP shows an increasing deviation with increasing number of complexed ligands. The stability constants of the 1:1 complexes agree within the uncertainties. These results are in good agreement with the solid-state structures of the C4-BPP and C5-BPP 1:1 complexes with Eu(III), which show no difference in the bond lengths. The stability constants of the 1:2 and 1:3 complexes differ by one and three orders of magnitude, respectively. C4-BPP features a directly attached ^{t}Bu group in comparison to C5-BPP (neopentyl group). The alkyl moieties are far away from the coordinating centre, excluding an electronic effect as a possible explanation for the observed differences in complex stabilities. These differences rather originate from a greater steric straining within the complex which is caused by the steric demand and limited flexibility of the ^{t}Bu moieties. With increasing coordination number, the steric hindrance of the C4-BPP molecules increases significantly, diminishing the overall stability of the resulting complex species. In case of C5-BPP, this effect is cushioned by the additional CH_2 groups which provide a flexible tool to decrease the spatial demand of the ^{t}Bu moieties.

Vibronic Side-band Spectroscopy of $[Cm(C4\text{-}BPP)_3]^{3+}$. To gain additional information on the complex structure vibronic side-band spectroscopy (VBS) is performed at the highest C4-BPP concentration of the titration series with $[Cm(C4\text{-}BPP)_3]$ being the dominating species. With this method functional groups coordinated to the central metal ion can be made visible through their characteristic vibrations. The obtained spectrum contains the zero phonon line, herein referred as ZPL, which originates from the Cm(III) $^6D'_{7/2} \rightarrow {}^8S'_{7/2}$ transition and the related side bands. Side bands occur due to changes in the dipole moment of the ligand field resulting from the excitation of the vibrational states of the examined metal ion.[36-39] The energy of the vibration is calculated relative to the ZPL according to equation (4).

$$E(vibration) = E(ZPL) - E(vibronic\ sideband) \quad \textbf{(4)}$$

The vibronic side bands of the $[Cm(C4\text{-}BPP_3]^{3+}$ complex species are depicted in Figure 7 (black). The ZPL is located at 611.7 nm. Two sidebands, at 970 cm^{-1} and 1420 cm^{-1} are obtained, which can be assigned to aromatic vibrations of the ligand. To assign the remaining bands, the structure of $[Cm(C4\text{-}BPP_3]^{3+}$ is optimized by DFT calculations and the vibronic side bands are calculated. The calculation (red, Figure 7) shows a band at 3374 cm^{-1}.[40, 41] This marks the N-H stretching vibration of the non-coordinated nitrogen atom. Unfortunately this bonds is too far away from the central metal ion to be detected. Furthermore the spectrum shows the absence of water in the first sphere of coordination due to the absence of a O-H stretching vibration located at around 3600 cm^{-1}.[40, 41] This emphasizes the dominating share of the $[Cm(C4\text{-}BPP)_3]^{3+}$ complex.

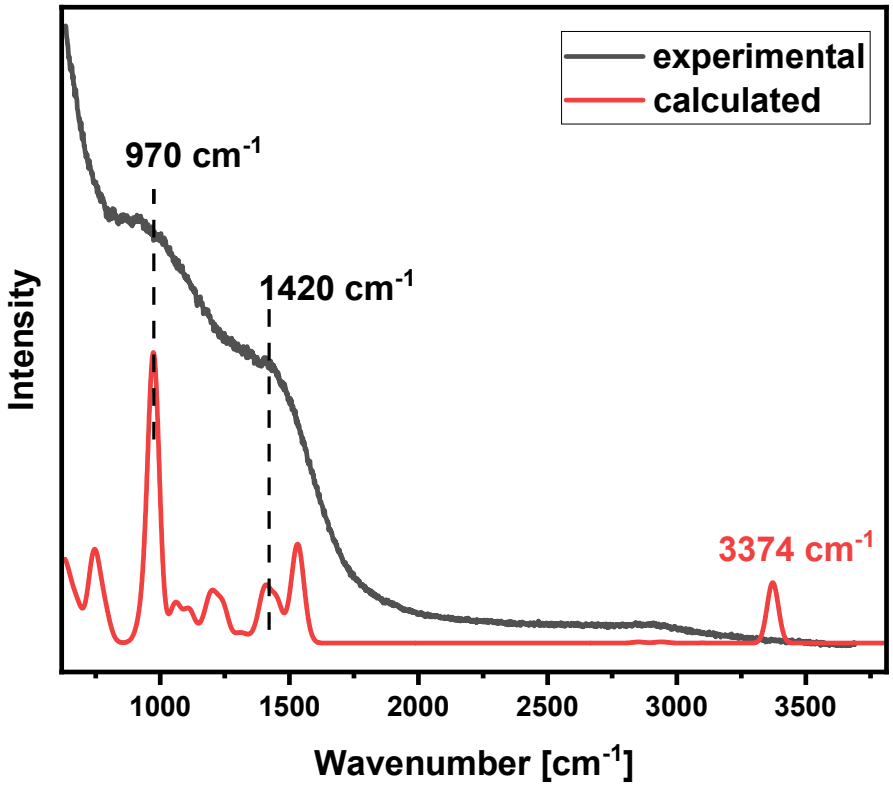

Figure 7: Comparison of the experimental and calculated VSB spectra of $[Cm(C4\text{-}BPP)_3]^{3+}$. $[Cm]_{ini}$ = $1.0 \bullet 10^{-7}$ mol/L. [C4-BPP] = $5.0 \bullet 10^{-2}$ mol/L.

Speciation studies of Eu(III) with C4-BPP. With respect to the differences in binding properties of 4f- and 5f-elements it is of interest to study Eu(III) in comparison to Cm (III). Eu(III) is dissolved in methanol containing 1.5 vol.% water and the concentration of C4-BPP is gradually increased. The normalized emission spectra resulting from the $^5D_0 \rightarrow {}^7F_1$ and $^5D_0 \rightarrow {}^7F_2$ transition are shown in Figure 8.

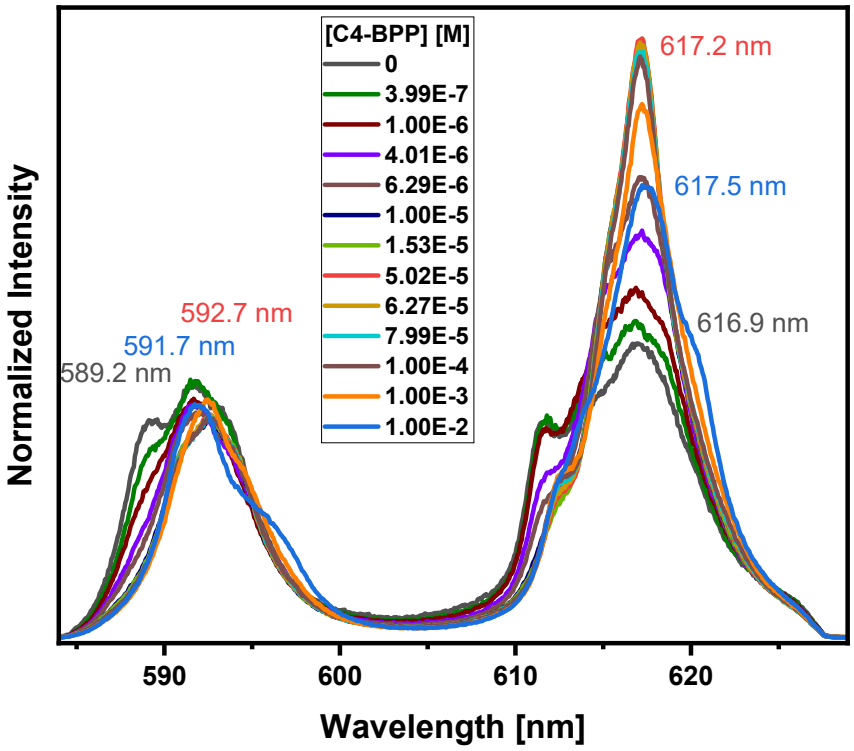

Figure 8: Normalized fluorescence spectra of Eu(III) in methanol containing 1.5 vol.% water as a function of the C4-BPP concentration. $[Eu(III)]_{ini} = 1.0 \bullet 10^{-6}$ mol/L, [C4-BPP] = (0 - 1.00) • 10^{-2} mol/L.

In absence of C4-BPP the solvent spectrum of Eu(III) in methanol containing 1.5 vol.% water is characterized by two emission bands at 589.2 ($^5D_0 \rightarrow {}^7F_1$) and 616.9 nm ($^5D_0 \rightarrow {}^7F_2$) (Figure 8) and a lifetime of 212 ± 11 µs. In addition the solvent spectrum shows an I($^5D_0 \rightarrow {}^7F_2$)/I($^5D_0 \rightarrow {}^7F_1$) ratio, herein after referred to as $^7F_2/{}^7F_1$ ratio, of 1. Increasing the C4-BPP concentration yields to a significant change of the $^5D_0 \rightarrow {}^7F_2$ transition with a new maximum at 617.2 nm. The $^7F_2/{}^7F_1$ ratio of 2.7 indicates the formation of a species with reduced symmetry in respect to the solvents species. Additional increase of the ligand concentration yields to further changes in intensity and shift of the emission bands (591.7 nm ($^5D_0 \rightarrow {}^7F_1$) and 617.5 nm ($^5D_0 \rightarrow {}^7F_2$)). The Eu(III) species distribution is performed, by peak deconvolution of the fluorescence spectra using the single component spectra (Figure S5) (for further details on peak deconvolution, see references).[2, 3]

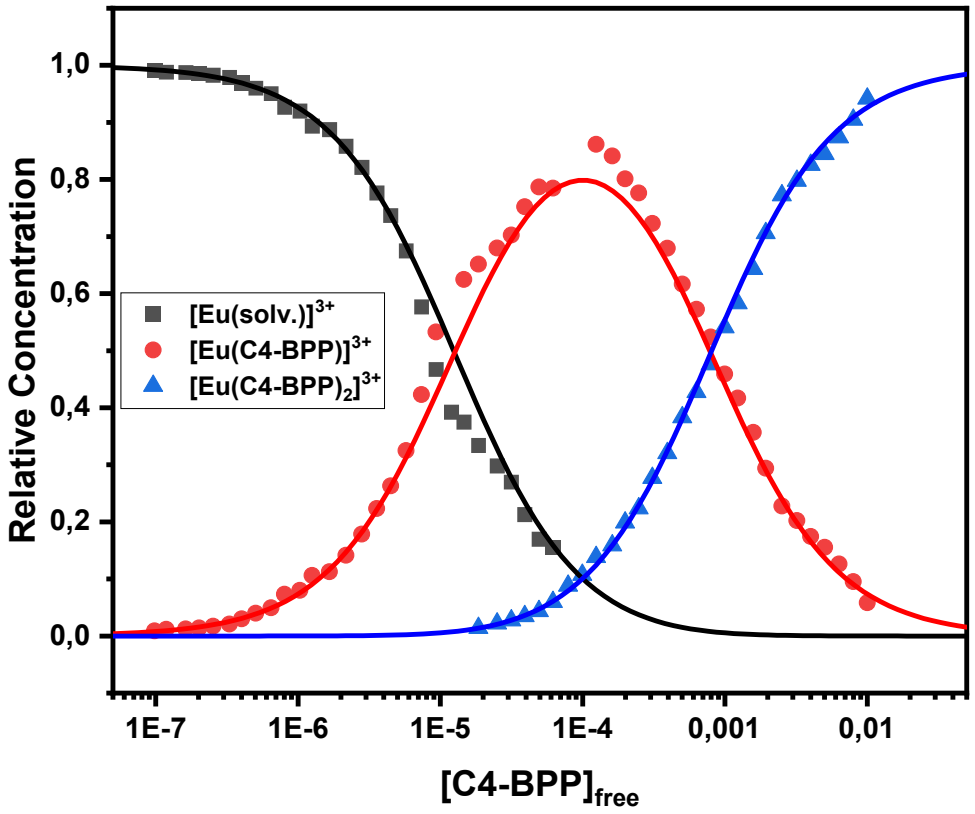

Figure 9: Relative Eu(III) species concentrations in methanol containing 1.5 vol.% water as a function of the free C4-BPP concentration. Symbols denote experimental data, while lines are calculated using log β'_1 = 4.9 and log β'_2 = 8.0. T = 293 K.

At low ligand concentrations the solvent species is the dominant species. The formation of $[Eu(C4\text{-}BPP)]^{3+}$ starts at $3.0 \cdot 10^{-7}$ mol/L C4-BPP and gradually increases until it evolves as the dominant species at $1.3 \cdot 10^{-5}$ mol/L ligand concentration. Above $4.0 \cdot 10^{-5}$ mol/L ligand, the $[Eu(C4\text{-}BPP)_2]^{3+}$ complex forms and is the prevailing species at $8.0 \cdot 10^{-4}$ mol/L. A lifetime of 2415 ± 120 µs is observed. According to equation (3) the conditional stability constants are calculated: $\beta'_1 = 4.9 \pm 0.2$ and $\beta'_2 = 8.0 \pm 0.4$. These values are significantly smaller than those for the Cm(III) 1:1 and 1:2 complexes ($\beta'_1 = 7.2 \pm 0.4$, $\beta'_2 = 10.1 \pm 0.5$). Additionally, the absence of a $[Eu(C4\text{-}BPP)_3]^{3+}$ complex shows the favored complexation of Cm(III) over Eu(III) under the given conditions. Since there are no reported values for Eu(III) and C5-BPP a comparison is not possible. Plotting the logarithm of $([Eu(C4\text{-}BPP)_n]^{3+}/[Eu(C4\text{-}BPP)_{n-1}]^{3+})$ as a function of the logarithm of the free C4-BPP concentration (Supporting Information, Figure 6) and applying equation (2) results in slopes of 1.00 ± 0.10 and 1.00 ± 0.01 for the $[Eu(C4\text{-}BPP)_n]^{3+}$ complexes (n = 1-2) respectively. This is in good agreement with the postulated complexation model and allocation of the complex species.

NMR Ln(III) complexes with C4-BPP. To get further insights into the interaction of C4-BPP with Ln(III) and An(III), various complexes are studied via NMR spectroscopy. In order to determine the NMR speciation, we firstly conducted NMR titration experiments for M(III) = Lu, Sm, La, Y with C4-BPP. An example is given in Figure 10, which displays the progression of the proton NMR at different Lu:L ratios. In total, the formation of three distinct complex species is observed. Additionally, the spectrum at Lu:L 1:4 shows the proton signals of the uncomplexed ligand, indicating the completion of the complexation. Consequently, we assume a stepwise complexation model from which each observed complex species can be assigned as $[Lu(C4\text{-}BPP)_n]^{3+}$ (n =1-3). Notably, the uncomplexed ligand shows substantial line broadening which is caused by an aggregation of the C4-BPP ligand molecules. As later studies indicate, the aggregation is suppressed in the presence of H^+ in the solution.

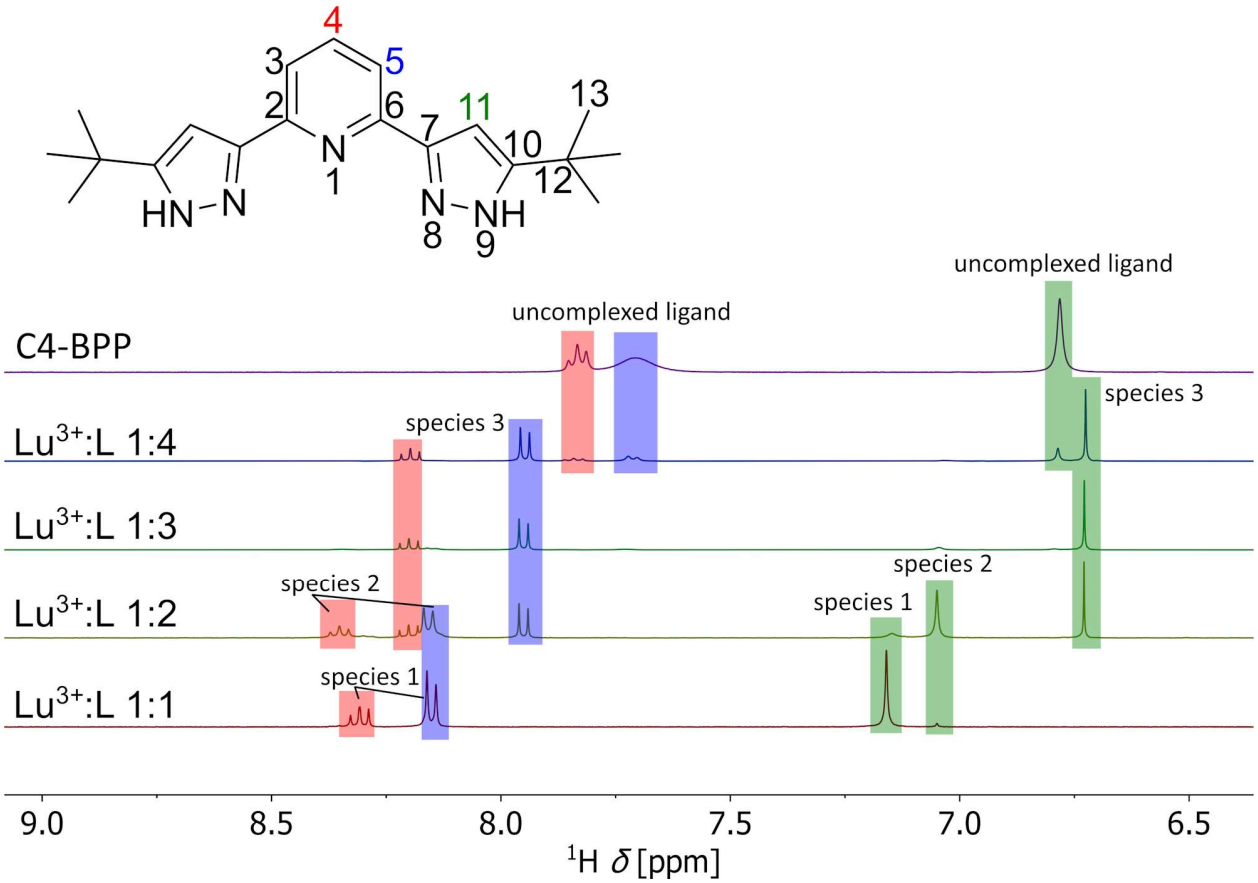

Figure 10: ^1H NMR spectra of the aromatic protons of C4-BPP at different Lu(III)-to-ligand ratios (Lu:L) in CD_3OD.

In the case of the metal ions, Y, La and Sm, a similar speciation is obtained (Figure S7-S9). However, a slight difference is observed in the stability of the complexes: La(III) requires at least 5.0 eq C4-BPP to form exclusively the $[La(C4\text{-}BPP)_3]^{3+}$ species; whereas $[Lu(C4\text{-}BPP)_3]^{3+}$ is dominantly present at 3.0 eq C4-BPP. This shows a clear correlation between the ionic radii and the complex stabilities along the Ln(III) series. With increasing ionic radius the stability decreases.

Using the acquired speciation data, $[M(C4\text{-}BPP)_3]^{3+}$ (M = Y, Sm, Lu, La) complexes are prepared and characterized using 1D (Figure S10-S13) and 2D NMR methods (S14-S16). Figure 11 displays the $^1H/^{15}N$ HMQC spectra of the 1:3 complexes in comparison to the uncomplexed ligand. All three chemically different nitrogen atoms are observed, which show long distance coupling with either H-11 or H-3/5. The

coordinated nitrogen atoms are found within a shift range of 35 ppm (N-1) and 30 ppm (N-8) in respect to the uncomplexed ligand. In contrast, the coordination impact is almost negligible for the non-coordinating N-9 nitrogen atom (Table 3).

It has to be noted, that the $^{1}H/^{15}N$ spectrum of the uncomplexed ligand is obtained in the presence of HOTf due to the ligand's aggregation in pure deuterated methanol. Nonetheless, the obtained chemical shifts fall within the range of literature known data of structurally related N-donor ligands. [14, 15, 19, 24, 26]

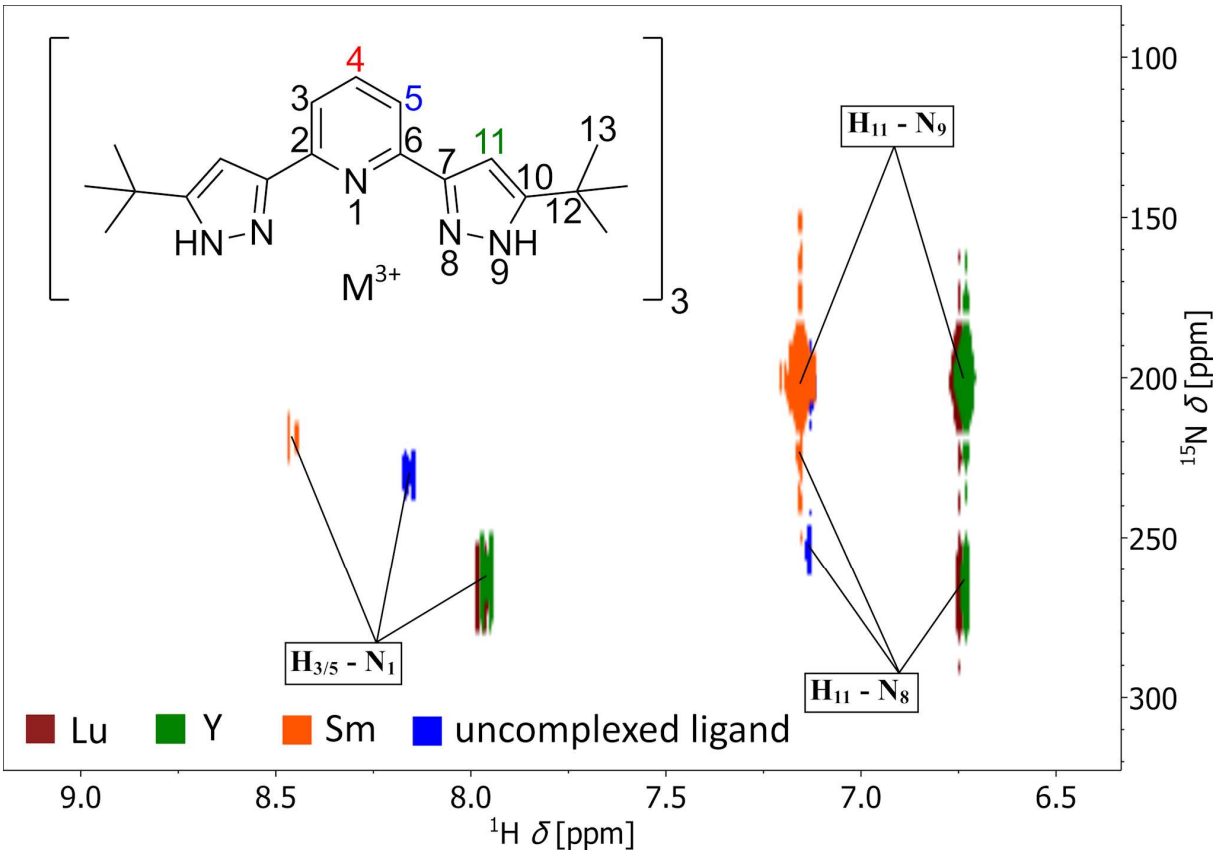

Figure 11: Overlay of ^{1}H, ^{15}N HMQC spectra of $[M(C4\text{-}BPP)_3](OTf)_3$ complexes (M = Y, Sm, Lu) and C4-BPP in CD_3OD.

Am complex with C4-BPP. As a representative of the trivalent An ions, the complexation of Am(III) with C4-BPP are studied using 1D and 2D NMR methods. Figure 12 shows the proton NMR spectrum of the Am complex at a M:L ratio of 1:3.5. The NMR spectrum exhibits in total four signals sets of which one can be assigned to the uncomplexed ligand. In comparison to the spectrum displayed in Figure 10, the signal set of the uncomplexed ligand differs significantly. This originates from an increased H^+ concentration in solution which inhibits the ligand aggregation. This effect can be reproduced by just adding HOTf to a solution containing C4-BPP in deuterated methanol (Figure 12, lower spectrum). The presence of H^+ ions can be traced back to residual HOTf from the $Am(OTf)_3$ stock solution which is carried over during the sample preparation. The residual H^+ ions have a decisive impact on the complex speciation as Figure 12 highlights. Against our expectation, three complex species are present in solution. These are identified by the singlet signals of the corresponding aromatic proton H-11 between 7.0 and 6.0 ppm. Based on a stepwise

complexation model, we assign the observed complex species to $[Am(C4\text{-}BPP)_n]^{3+}$ (n = 1-3). DOSY measurements proofs the presence of three distinct complexes (Figure S17). Furthermore, a titration experiment shows that the proton signal at 6.76 ppm corresponds to the 1:1, the signal at 6.50 ppm to the 1:2 and the signal at 6.09 ppm to the 1:3 complex (Figure S18). Additional NMR experiments involving the Ln(III) complex speciation in presence of HOTf confirm the strong impact of H^+ ions on the complexation (Figure S19).

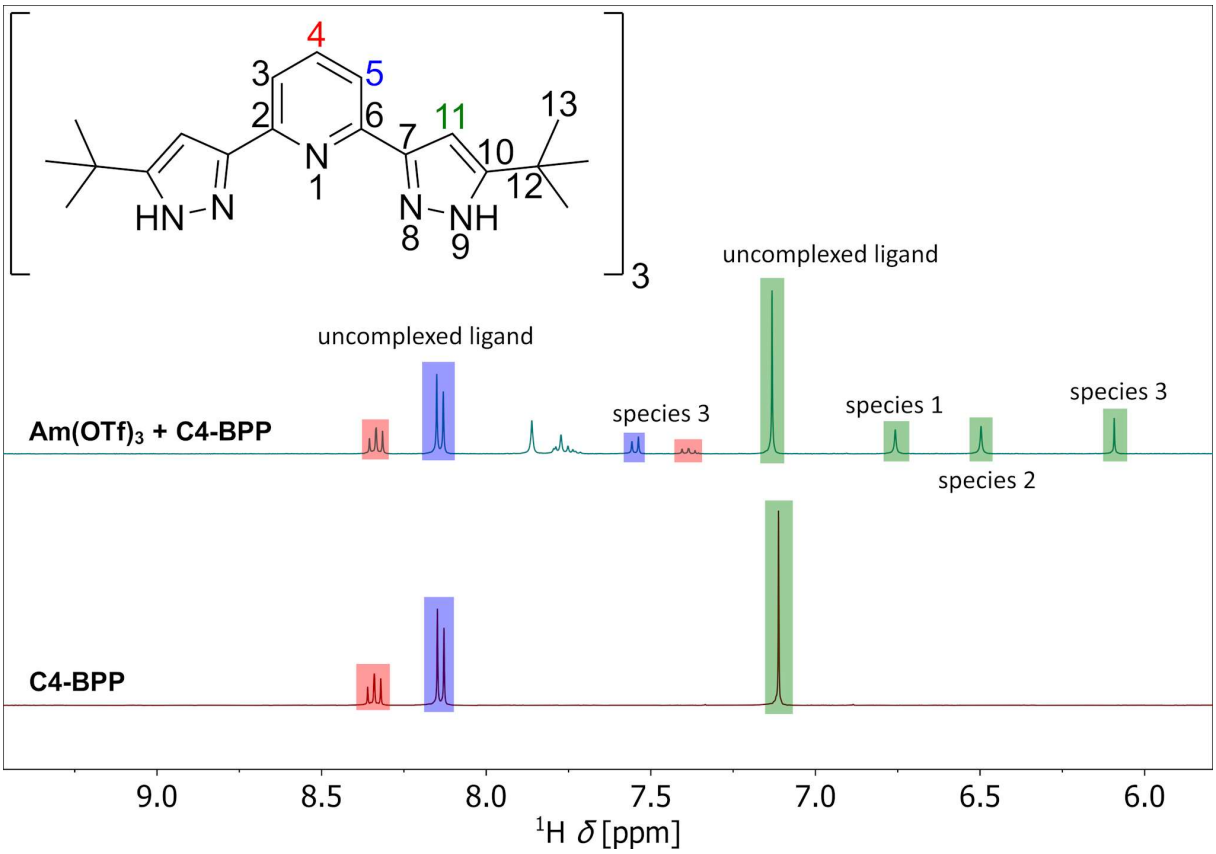

Figure 12: ^1H NMR Spectrum of the aromatic region of C4-BPP in presence of $Am(OTf)_3$ (upper spectrum) and HOTf (lower spectrum) in CD_3OD.

The complex mixture is further characterized by ^1H ^{15}N-HMQC measurement (see Figure 13). ^{15}N signals are found between -10 to +10 ppm for the coordinating nitrogen atoms N-8 and N-1 and around 210 ppm for the non-coordinating nitrogen atom N-9. In comparison to the ^{15}N shifts of the respective Ln(III) complexes, Am(III) shows a pronounced upfield shift of about 270 – 280 ppm for the coordinating nitrogen donor atoms (Table 3). These strong shifts can not only be attributed to the paramagnetism of Am(III) because Sm(III), which is comparable in paramagnetism, shows similar shifts as the diamagnetic Lu(III) and Y(III). Therefore, this pronounced shift is related to a difference in the M(III)-N interaction. The interaction between Ln(III) ions and ligands is generally considered to be driven mainly by electrostatic forces. Consequently, a change of the coordination mode includes a higher fraction of covalence in the Am(III)-N interaction. This is in good agreement with literature data where shifts up to 300 ppm of Am(III) complexes of other N-donor ligands in respect to the Ln(III) complexes were observed.[14, 15, 19, 24] Furthermore it must be highlighted that the chemical shifts of the coordinated nitrogen atoms are almost

identical for the 1:1 and 1:3 complex, which resembles that the observed shifts are independent of the complex structure as well as the complex stoichiometry. The small deviation may be a result from slightly different bond lengths and bond angle.

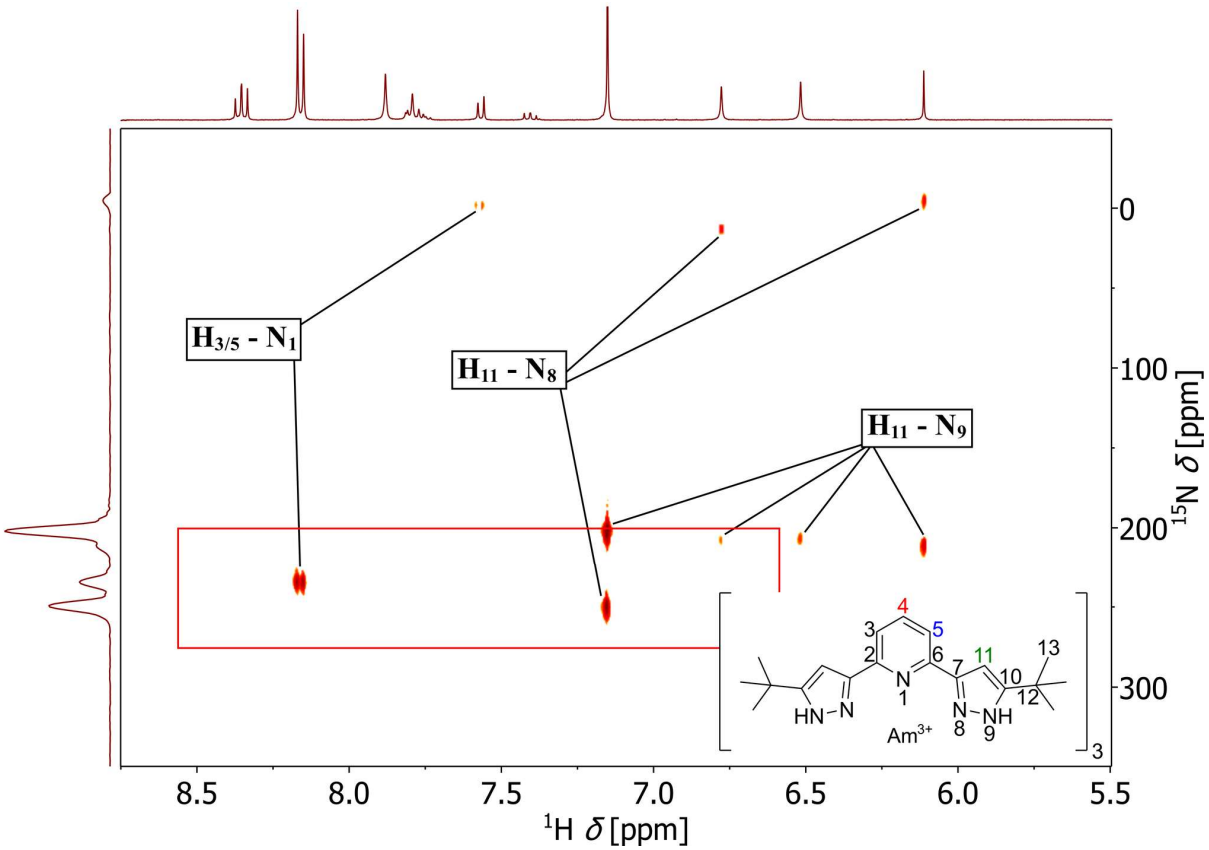

Figure 13: ^{1}H, ^{15}N HMQC spectrum of the $[Am(C4\text{-}BPP)_n]^{3+}$ (n = 1-3) complexes in CD_3OD. The highlighted red box shows the range of chemical shifts observed for the Ln(III) complexes.

Table 3: Chemical shifts of the nitrogen atoms in $M(C4\text{-}BPP)_n(OTf)_3$ (n =3) complexes and in the uncomplexed ligand.

Metal	N-1	N-8	N-9
none	230[a]	254[a]	202[a]
Y^{3+}	263	265	200
Sm^{3+}	218	224	200
Lu^{3+}	265	267	200
Am^{3+} (1:3)	-3	-6	212
Am^{3+} (1:2)	-	-	207
Am^{3+} (1:1)	-	13	207

[a] Labeled values are taken from spectra with 1.5 mol/L HOTf.

Conclusion

The present work aims to deepen the understanding of the bonding properties of An(III) and Ln(III) with N-donor ligands like C4-BPP.

Speciation studies using TRLFS show the formation of $[Cm(C4\text{-}BPP)_n]^{3+}$ (n = 1-3) and $[Eu(C4\text{-}BPP)_n]^{3+}$ (n = 1-2) in methanol containing 1.5 vol.% water. Stability constants of the Cm(III) complexes are by two orders of magnitude larger ($\beta'_1 = 7.2$, $\log \beta'_2 = 10.1$, $\log \beta'_3 = 11.8$) than Eu(III) complexes ($\log \beta'_1 = 4.9$; $\log \beta'_2 = 8.0$). Additionally, a 1:3 Eu(III) complex is not observed under the given conditions. This indicates a stronger ligand-metal ion interaction in the An(III) complex compared to the respective Ln(III) complex. Cm values are lower in the current system compared to previously studied C5-BPP ligand because of the steric demand of the ^{t}Bu moieties comparing to the neopentyl groups.

NMR studies show the formation of $[M(C4\text{-}BPP)_n]^{3+}$ (n = 1-3) for Am(III) and Ln(III) ions. Additionally, the speciation is dependent on the concentration of H^+ in solution. $^1H/^{15}N$ HMQC analysis provided insights into the metal ion- nitrogen interaction. The data analysis suggests a different bonding mode in the Am(III) complex in respect to comparable Ln(III) complexes.[14, 15] Consequently, we conclude a higher fraction of covalence in the Am(III)-N interaction. This is consistent with existing literature data.[14, 15, 19, 24]

Supporting Information

CCDC 2328668 contains the supplementary crystallographic data for this paper. The data can be obtained free of charge from The Cambridge Crystallographic Data Centre via www.ccdc.cam.ac.uk/structures.

Acknowledgements

This work was supported by the German Federal Ministry for Economic Affairs and Climate Action (BMUV) under contract number 02E11921B and the German Federal Ministry of Education and Research (BMBF) under contract numbers 02NUK059A and 02NUK059C.

References

[1] J. Rydberg, M. Cox, C. Musikas, Choppin, G. R., *Solvent Extraction Principles and Practice*, Marcel Dekker, New York, **2004**.

[2] Weßling, P., Trumm, M., Macerata, E., Ossola, A., Mossini, E., Gullo, M. C., Arduini, A., Casnati, A., Mariani, M., Adam, C., Geist, A., Panak, P. J., Activation of the Aromatic Core of 3,3′-(Pyridine-2,6-diylbis(1H-1,2,3-triazole-4,1-diyl))bis(propan-1-ol) — Effects on Extraction Performance, Stability Constants, and Basicity, *Inorg. Chem.* **2019**, *58*, 14642-14651. DOI: 10.1021/acs.inorgchem.9b02325

[3] Weßling, P., Trumm, M., Geist, A., Panak, P. J., Stoichiometry of An(iii)–DMDOHEMA complexes formed during solvent extraction, *Dalton Transactions* **2018**, *47*, 10906-10914. DOI: 10.1039/C8DT02504E

[4] Panak, P. J., Geist, A., Complexation and Extraction of Trivalent Actinides and Lanthanides by Triazinylpyridine N-Donor Ligands, *Chem. Rev.* **2013**, *113*, 1199-1236. DOI: 10.1021/cr3003399

[5] Cotton, S. A., *Lanthanide and Actinide Chemistry*, John Wiley & Sons, West Sussex, **2006**.

[6] Zhu, Y., Chen, J., Jiao, R., Extraction of Am(III) and Eu(III) from Nitrate Solution with Purified Cyanex 301, *Solvent Extraction and Ion Exchange* **1996**, *14*, 61-68. DOI: 10.1080/07366299608918326

[7] Modolo, G., Odoj, R., SYNERGISTIC SELECTIVE EXTRACTION OF ACTINIDES(III) OVER LANTHANIDES FROM NITRIC ACID USING NEW AROMATIC DIORGANYLDITHIOPHOSPHINIC ACIDS AND NEUTRAL ORGANOPHOSPHORUS COMPOUNDS, *Solvent Extraction and Ion Exchange* **1999**, *17*, 33-53. DOI: 10.1080/07360299908934599

[8] Kolarik, Z., Mullich, U., Gassner, F., EXTRACTION OF Am(lll) AND Eu(lll) NITRATES BY 2-6-DI-(5,6-DIPROPYL-1,2,4-TRIAZIN-3-YL)PYRIDINES 1, *Solvent Extraction and Ion Exchange* **1999**, *17*, 1155-1170. DOI: 10.1080/07366299908934641

[9] Drew, M. G. B., Foreman, M. R. S. J., Hill, C., Hudson, M. J., Madic, C., 6,6′-bis-(5,6-diethyl-[1,2,4]triazin-3-yl)-2,2′-bipyridyl the first example of a new class of quadridentate heterocyclic extraction reagents for the separation of americium(III) and europium(III), *Inorg. Chem. Commun.* **2005**, *8*, 239-241. DOI: 10.1016/j.inoche.2004.12.017

[10] Geist, A., Panak, P. J., Recent Progress in Trivalent Actinide and Lanthanide Solvent Extraction and Coordination Chemistry with Triazinylpyridine N Donor Ligands, *Solvent Extraction and Ion Exchange* **2021**, *39*, 128-151. DOI: 10.1080/07366299.2020.1831235

[11] Bremer, A., Ruff, C. M., Girnt, D., Müllich, U., Rothe, J., Roesky, P. W., Panak, P. J., Karpov, A., Müller, T. J. J., Denecke, M. A., Geist, A., 2,6-Bis(5-(2,2-dimethylpropyl)-1H-pyrazol-3-yl)pyridine as a Ligand for Efficient Actinide(III)/Lanthanide(III) Separation, *Inorg. Chem.* **2012**, *51*, 5199-5207. DOI: 10.1021/ic3000526

[12] Bremer, A., Geist, A., Panak, P. J., Complexation of Cm(III) and Eu(III) with 2,6-bis(5-(2,2-dimethylpropyl)-1H-pyrazol-3-yl)pyridine and 2-bromohexanoic acid studied by time-resolved laser fluorescence spectroscopy, *Radiochimica Acta* **2013**, *101*, 285-292. DOI: 10.1524/ract.2013.2037

[13] Bremer, A., Müllich, U., Geist, A., Panak, P. J., Influence of the solvent on the complexation of Cm(iii) and Eu(iii) with nPr–BTP studied by time-resolved laser fluorescence spectroscopy, *New Journal of Chemistry* **2015**, *39*, 1330-1338. DOI: 10.1039/C4NJ01900H

[14] Adam, C., Kaden, P., Beele, B. B., Müllich, U., Trumm, S., Geist, A., Panak, P. J., Denecke, M. A., Evidence for covalence in a N-donor complex of americium(iii), *Dalton Transactions* **2013**, *42*, 14068-14074. DOI: 10.1039/C3DT50953B

[15] Adam, C., Beele, B. B., Geist, A., Müllich, U., Kaden, P., Panak, P. J., NMR and TRLFS studies of Ln(iii) and An(iii) C5-BPP complexes, *Chemical Science* **2015**, *6*, 1548-1561. DOI: 10.1039/C4SC03103B

[16] Street, K., Jr., Seaborg, G. T., The Separation of Americium and Curium from the Rare Earth Elements, *Journal of the American Chemical Society* **1950**, *72*, 2790-2792. DOI: 10.1021/ja01162a530
[17] Cooper, S., Kaltsoyannis, N., Covalency in AnCl3 (An = Th–No), *Dalton Transactions* **2021**, *50*, 1478-1485. DOI: 10.1039/D0DT03699D
[18] Kaltsoyannis, N., Does Covalency Increase or Decrease across the Actinide Series? Implications for Minor Actinide Partitioning, *Inorg. Chem.* **2013**, *52*, 3407-3413. DOI: 10.1021/ic3006025
[19] Adam, C., Rohde, V., Müllich, U., Kaden, P., Geist, A., Panak, P. J., Geckeis, H., Comparative NMR Study of nPrBTP and iPrBTP, *Procedia Chemistry* **2016**, *21*, 38-45. DOI: 10.1016/j.proche.2016.10.006
[20] Girnt, D., Roesky, P. W., Geist, A., Ruff, C. M., Panak, P. J., Denecke, M. A., 6-(3,5-Dimethyl-1H-pyrazol-1-yl)-2,2′-bipyridine as Ligand for Actinide(III)/Lanthanide(III) Separation, *Inorg. Chem.* **2010**, *49*, 9627-9635. DOI: 10.1021/ic101309j
[21] Bremer, A., Geist, A., Panak, P. J., Complexation of Cm(iii) with 6-(5,6-dipentyl-1,2,4-triazin-3-yl)-2,2′-bipyridine studied by time resolved laser fluorescence spectroscopy, *Dalton Transactions* **2012**, *41*, 7582-7589. DOI: 10.1039/C2DT30541K
[22] Beele, B. B., Rüdiger, E., Schwörer, F., Müllich, U., Geist, A., Panak, P. J., A TRLFS study on the complexation of novel BTP type ligands with Cm(iii), *Dalton Transactions* **2013**, *42*, 12139-12147. DOI: 10.1039/C3DT50536G
[23] Beele, B. B., Skerencak-Frech, A., Stein, A., Trumm, M., Wilden, A., Lange, S., Modolo, G., Müllich, U., Schimmelpfennig, B., Geist, A., Panak, P. J., 2,6-Bis(5,6-diisopropyl-1,2,4-triazin-3-yl)pyridine: a highly selective N-donor ligand studied by TRLFS, liquid–liquid extraction and molecular dynamics, *New Journal of Chemistry* **2016**, *40*, 10389-10397. DOI: 10.1039/C6NJ02657E
[24] Galluccio, F., Macerata, E., Weßling, P., Adam, C., Mossini, E., Panzeri, W., Mariani, M., Mele, A., Geist, A., Panak, P. J., Insights into the Complexation Mechanism of a Promising Lipophilic PyTri Ligand for Actinide Partitioning from Spent Nuclear Fuel, *Inorg. Chem.* **2022**, *61*, 18400-18411. DOI: 10.1021/acs.inorgchem.2c02332
[25] Weßling, P., Trumm, M., Sittel, T., Geist, A., Panak, P. J., Spectroscopic investigation of the different complexation and extraction properties of diastereomeric diglycolamide ligands, *Radiochimica Acta* **2022**, *110*, 291-300. DOI: 10.1515/ract-2021-1134
[26] Sittel, T., Weßling, P., Großmann, D., Engels, E., Geist, A., Panak, P. J., Spectroscopic investigation of the covalence of An(iii) complexes with tetraethylcarboxamidopyridine, *Dalton Transactions* **2022**, *51*, 8028-8035. DOI: 10.1039/D2DT00757F
[27] Becke, A. D., Density-functional exchange-energy approximation with correct asymptotic behavior, *Physical Review A* **1988**, *38*, 3098-3100. DOI: 10.1103/PhysRevA.38.3098
[28] Perdew, J. P., Density-functional approximation for the correlation energy of the inhomogeneous electron gas, *Physical Review B* **1986**, *33*, 8822-8824. DOI: 10.1103/PhysRevB.33.8822
[29] Weigend, F., Ahlrichs, R., Balanced basis sets of split valence, triple zeta valence and quadruple zeta valence quality for H to Rn: Design and assessment of accuracy, *Physical Chemistry Chemical Physics* **2005**, *7*, 3297-3305. DOI: 10.1039/B508541A
[30] *TURBOMOLE V7.5*, a development of University of Karlsruhe and Forschungszentrum Karlsruhe GmbH, 1989-2007, TURBOMOLE GmbH, since 2007.
[31] Küchle, W., Dolg, M., Stoll, H., Preuss, H., Energy‐adjusted pseudopotentials for the actinides. Parameter sets and test calculations for thorium and thorium monoxide, *The Journal of Chemical Physics* **1994**, *100*, 7535-7542. DOI: 10.1063/1.466847
[32] Kimura, T., Choppin, G. R., Kato, Y., Yoshida, Z., Determination of the Hydration Number of Cm(III) in Various Aqueous Solutions, *Radiochimica Acta* **1996**, *72*, 61-64. DOI: 10.1524/ract.1996.72.2.61
[33] Skanthakumar, S., Antonio, M. R., Wilson, R. E., Soderholm, L., The Curium Aqua Ion, *Inorg. Chem.* **2007**, *46*, 3485-3491. DOI: 10.1021/ic061798b

[34] Bauer, N., Smith, V. C., MacGillivray, R. T. A., Panak, P. J., Complexation of Cm(iii) with the recombinant N-lobe of human serum transferrin studied by time-resolved laser fluorescence spectroscopy (TRLFS), *Dalton Transactions* **2015**, *44*, 1850-1857. DOI: 10.1039/C4DT03403A

[35] Stumpf, T., Marques Fernandes, M., Walther, C., Dardenne, K., Fanghänel, T., Structural characterization of Am incorporated into calcite: A TRLFS and EXAFS study, *J. Colloid Interface Sci.* **2006**, *302*, 240-245. DOI: 10.1016/j.jcis.2006.06.010

[36] Freed, S., Spectra of Ions in Fields of Various Symmetry in Crystals and Solutions, *Reviews of Modern Physics* **1942**, *14*, 105-111. DOI: 10.1103/RevModPhys.14.105

[37] Iben, I. E., Stavola, M., Macgregor, R. B., Zhang, X. Y., Friedman, J. M., Gd3+ vibronic side band spectroscopy. New optical probe of Ca2+ binding sites applied to biological macromolecules, *Biophys. J.* **1991**, *59*, 1040-1049. DOI: 10.1016/S0006-3495(91)82319-0

[38] Chodos, S. L., Satten, R. A., Model calculation of vibronic sidebands in Cs2UBr6, *The Journal of Chemical Physics* **2008**, *62*, 2411-2417. DOI: 10.1063/1.430767

[39] Ewald, H., Die Analyse und Deutung der Neodymsalzspektren, *Annalen der Physik* **1939**, *426*, 209-236. DOI: 10.1002/andp.19394260302

[40] Nakamoto, K., *Infrared and Raman Spectra of Inorganic and Coordination Compounds, Applications in Coordination, Organometallic, and Bioinorganic Chemistry*, John Wiley & Sons, **2009**.

[41] Socrates, G., *Infrared and Raman Characteristic Group Frequencies: Tables and Charts*, John Wiley & Sons, **2004**.